Structures of Two Streptococcal Superantigens Bound to TCR β Chains Reveal Diversity in the Architecture of T Cell Signaling Complexes

Eric J. Sundberg,[1] Hongmin Li,[1,5] Andrea S. Llera,[1,6]
John K. McCormick,[2] José Tormo,[1,7]
Patrick M. Schlievert,[2] Klaus Karjalainen,[3]
and Roy A. Mariuzza[1,4]
[1]Center for Advanced Research in Biotechnology
W.M. Keck Laboratory for Structural Biology
University of Maryland Biotechnology Institute
9600 Gudelsky Drive
Rockville, Maryland 20850
[2]Department of Microbiology
University of Minnesota Medical School
Minneapolis, Minnesota 55455
[3]Basel Institute for Immunology
Grenzacherstrasse 487
CH-4005 Basel
Switzerland

Summary

Superantigens (SAGs) crosslink MHC class II and TCR molecules, resulting in an overstimulation of T cells associated with human disease. SAGs interact with several different surfaces on MHC molecules, necessitating the formation of multiple distinct MHC-SAG-TCR ternary signaling complexes. Variability in SAG-TCR binding modes could also contribute to the structural heterogeneity of SAG-dependent signaling complexes. We report crystal structures of the streptococcal SAGs SpeA and SpeC in complex with their corresponding TCR β chain ligands that reveal distinct TCR binding modes. The SpeC-TCR β chain complex structure, coupled with the recently determined SpeC-HLA-DR2a complex structure, provides a model for a novel T cell signaling complex that precludes direct TCR-MHC interactions. Thus, highly efficient T cell activation may be achieved through structurally diverse strategies of TCR ligation.

Introduction

Superantigens (SAGs) are immunostimulatory and disease-associated proteins of bacterial or viral origin that bind simultaneously to major histocompatibility complex (MHC) class II and T cell receptor (TCR) molecules on the surfaces of antigen-presenting cells and T lymphocytes [1, 2]. Contrary to processed antigenic peptides, SAGs bind to MHC molecules outside of the peptide binding groove and interact with TCR Vβ domains, resulting in the stimulation of a large fraction (up to 5%–20%) of the T cell population. SAGs have been implicated in the pathogenesis of a number of human diseases, including toxic shock syndrome, food poisoning [3, 4], and several autoimmune disorders [5], such as Crohn's disease [6] and type I diabetes [7]. Although all known bacterial SAGs share a conserved three-dimensional fold, their interaction with MHC molecules and stimulation of T cells is highly variable, depending, to varying degrees, on the biochemical and structural states of MHC molecules on the cell surface [8], the ability of certain SAGs to coordinate zinc atoms [9, 10], and the sequence and structure of TCR Vβ domains expressed on the T cell surface.

The complexes formed between SAGs and MHC molecules have been shown to be structurally diverse. The MHC molecule presents two general surfaces for SAG docking, including a low-affinity site ($K_D \approx 10^{-5}$ M) on the conserved α chain and a high-affinity site ($K_D \approx 10^{-7}$ M) on the polymorphic β chain. Structural examples of SAGs bound to both MHC binding sites exist. Crystal structures of complexes formed by staphylococcal enterotoxin B (SEB) [11] and toxic shock syndrome toxin-1 (TSST-1) [12] with HLA-DR1 have shown that SAG binding to the MHC α chain can be accomplished through two distinct, yet overlapping, binding sites. This results in either no interactions with the bound antigenic peptide, as in the case of SEB, or partial occlusion of the surface of the peptide normally exposed to TCR, as for TSST-1. Two examples of SAGs bound to the high-affinity β chain site of MHC molecules suggest that binding to this side of the MHC molecule may be less variable. In these complexes, streptococcal pyrogenic exotoxin C (SpeC) in complex with HLA-DR2a [13] and SEH bound to HLA-DR1 [14], both SAGs coordinate a zinc ligand and interact with the antigenic peptide in a similar fashion. Further complicating the structural description of SAG-MHC interactions is the finding that some SAGs, such as SEA, have been shown biochemically to bind at both the high- and low-affinity sites [9, 15, 16].

In order to crosslink MHC and TCR molecules, all SAGs, regardless of their binding mode with MHC, interact with the Vβ domain of the TCR. SAGs bind their Vβ ligands with relatively low affinity ($K_D \approx 10^{-4}$ M–10^{-6} M) [2]. TCR specificity is also generally low, as most SAGs are specific only to Vβ domains and not to Vβ-Dβ-Jβ junctional sequences or Vα segments, allowing a single SAG species to stimulate such disproportionately large numbers of T cells and induce the massive cytokine release associated with SAG-mediated illnesses [2–4, 17]. To date, crystal structures involving only a single TCR β chain (mouse Vβ8.2) in complex with several SAGs, including SEC2 [18], SEC3 [18], and SEB [19],

have been determined. In all of these complexes, the SAG interacts predominantly with residues from the second complementarity-determining region (CDR2), the third framework region (FR3), and, to a lesser extent, the hypervariable region 4 (HV4) of the TCR β chain. The orientations of SEC2, SEC3, and SEB, when bound to the TCR β chain, are virtually identical.

A structural model of the TCR-SEB-MHC ternary complex, produced by assembling the various bimolecular structures involved, suggests that SEB acts as a wedge between the MHC α chain and the TCR β chain [19], causing a rotation of the TCR about the interface between the Vα CDR2 loop and the MHC β α helix in the TCR-peptide/MHC complex [20, 21] and effectively preventing the antigenic peptide and most of the CDR loops from making any specific interactions within the ternary complex. This model also predicts that at least some contacts between the MHC β and TCR α chains remain. Due to the variability in complex formation between SAGs and MHC molecules, the TCR-SEB-MHC ternary complex model cannot, by definition, represent accurately the structures of TCR-SAG-MHC complexes for those SAGs that bind differently to MHC, even if there exists only a single binding mode for SAG-TCR interactions. Although the SAG-TCR β chain complex structures determined to date have revealed a single binding mode, different SAGs bind to distinct groups of TCR Vβ subsets, with certain SAGs having the ability to bind many different Vβ domains, while others are more restricted in their Vβ domain specificity. Thus, it is likely that there exist multiple SAG-TCR binding modes. With variability in complex formation on both the MHC and TCR sides of the SAG crosslinking reaction, the number of distinct ternary complexes could be quite large.

To better understand the structural basis for the activation of T cells by bacterial SAGs, we have determined the structures of two SAGs from *Streptococcus pyogenes*, SpeA and SpeC, in complex with their specific TCR β chain ligands, mouse Vβ8.2 (mVβ8.2) and human Vβ2.1 (hVβ2.1), respectively. Together, SpeA and SpeC are associated with nearly all cases of streptococcal toxic shock syndrome [22]. While the structure of the SpeA-mVβ8.2 complex is very similar to structures of this TCR β chain complexed with SAGs from *Staphylococcus aureus* [18, 19], differences in the number and types of intermolecular contacts in the common binding interface, as well as the involvement of the CDR1 loop, distinguish the SpeA binding mode. The SpeC-hVβ2.1 complex structure, conversely, reveals a completely different set of SAG-TCR interactions, involving a much more extensive buried surface area and numerous specific interactions between SpeC residues and all three of the TCR β chain CDRs, as well as HV4. Coupled with the SpeC-HLA-DR2a complex structure [13], in which SpeC binds to the high-affinity MHC β chain site, we provide an alternative model for TCR-SAG-MHC ternary complex formation bearing little resemblance to that of SEB and show that wide variations are possible in the specific geometry of TCR engagement by SAG-MHC ligands that are nevertheless compatible with highly efficient T cell activation comparable to that by specific peptide/MHC complexes.

Results

Overview of the SpeC-hVβ2.1 and SpeA-mVβ8.2 Structures

We have determined the structure of the complex between SpeC, in which the histidine residue at position 35 was mutated to an alanine (SpeC H35A) and the human Vβ2.1Dβ2.1Jβ2.3Cβ2 TCR β chain, hVβ2.1. While the SpeC wild-type and mutant proteins bind the TCR β chain with similar affinities ($K_D \approx 2 \times 10^{-5}$ M; data not shown), only the SpeC variant crystallized with hVβ2.1, much as in the case of the SpeC-HLA-DR2a complex [13]. The structure of the complex was determined by molecular replacement using wild-type SpeC [10] as a search model, combined with manual chain tracing of TCR β chains in $2F_o - F_c$ electron density maps calculated with phases from four SpeC molecules in the asymmetric unit (see Experimental Procedures). There are four SpeC molecules and two TCR β chain molecules per asymmetric unit in the final model. Although noncrystallographic symmetry, crystal packing constraints, and electron density allude to the presence of two additional TCR β chain molecules in the crystal that form similar heterodimeric complexes with the two unbound SpeC molecules as those that are bound (in the final model), they were not built into the final model because their inclusion did not improve the overall refinement statistics. The SpeC mutation site, H35A, is located in neither the β-SpeC nor the SpeC-SpeC interface in the crystal. Crystallographic data collection and structure refinement statistics are summarized in Table 1. Although the data integrates well to a nominal resolution of 3.0 Å, as shown by the statistics of the highest resolution shell, 3.11–3.0 Å, diffraction intensities beyond this resolution degraded precipitously to such an extent that the inclusion of any higher diffraction data would only increase uncertainty in the model. A large degree of disorder in the crystal radiates from the interface of the first β-SpeC complex (as evidenced by the increasingly higher B factor values for peripheral molecules) and is the likely reason for our inability to model all of the TCR β chain molecules and the relatively high R factor values. While this disorder results in an unavoidably underdetermined overall crystal structure, the first β-SpeC complex in the asymmetric unit is well ordered throughout, and, thus, all further analysis and discussion is limited to this particular binary complex. Figure 1A shows electron density from a composite annealed omit map in this β-SpeC interface region, revealing well defined atomic positions for both main chain and side chain atoms.

We also solved the structure of SpeA, in which a free cysteine at position 90 has been mutated to a serine (SpeA C90S) complexed with the 14.3.d TCR β chain (mouse Vβ8.2Jβ2.1Cβ1, mVβ8.2) in two forms, with and without zinc, since a potential zinc binding site for SpeA has been described [23]. Although the wild-type and mutant SpeA molecules bind TCR β with similar affinities ($K_D \approx 6 \times 10^{-6}$ M; [24] and data not shown), attempts to crystallize the wild-type β-SpeA complex in the presence of reducing agent resulted only in poorly diffracting crystals. Mutation of the free cysteine in SpeA allowed the growth of crystals in the absence of reducing agent and resulted in significant improvement in diffraction

Table 1. Crystal Data Collection and Structure Refinement Statitics

	β-SpeC		β-SpeA (apo)		β-SpeA (zinc-soaked)
Data Collection					
Space group	P2₁		P2₁		P2₁
Unit cell dimensions					
a (Å)	57.4		71.4		71.7
b (Å)	146.8		83.3		83.7
c (Å)	135.7		93.6		93.9
β (°)	98.6		91.7		91.7
Molecules per asymmetric unit	4 SpeC/4 hVβ2.1		2 SpeA/2 mVβ8.2		2 SpeA/2 mVβ8.2
Resolution (Å)	3.0		2.8		2.5
Mosaicity (°)	0.4		0.6		0.5
Observations	158,446		80,520		115,588
Unique reflections	43,729		26,926		37,614
Completeness (%)	97.8 (96.5)[a]		99.1 (99.8)		96.7 (77.9)
Mean I/σ (I)	16.0 (6.5)		9.6 (3.6)		10.3 (1.4)
R_{sym}[b] (%)	5.0 (20.7)		12.1 (37.3)		10.7 (48.1)
Refinement					
R_{work}[c] (%)	32.6 (35.7)		23.2 (39.7)		22.1 (32.0)
R_{free}[c] (%)	33.5 (36.2)		27.8 (45.9)		26.2 (38.3)
Protein residues	1200		914		913
Water molecules	0		181		316
Zinc atoms	0		0		6
Average B factors					
SpeC (1)	59.1	SpeA (1)	41.7	SpeA (1)	42.2
SpeC (2)	79.9	SpeA (2)	38.0	SpeA (2)	35.4
SpeC (3)	60.1	Vβ (1)	26.6	Vβ (1)	25.2
SpeC (4)	77.2	Cβ (1)	53.8	Cβ (1)	52.3
Vβ (1)	79.7	Vβ (2)	26.9	Vβ (2)	24.6
Cβ (1)	84.2	Cβ (2)	52.7	Cβ (2)	52.5
Vβ (2)	108.2	H₂O	29.9	H₂O	34.5
Cβ (2)	123.0			Zinc	53.1
Rms deviations from ideality					
Bonds (Å)	0.011		0.007		0.007
Angles (°)	1.99		1.34		1.28
Ramachandran plot statistics					
Core (%)	62.5		84.7		85.6
Allowed (%)	28.0		14.2		13.5
Generous (%)	8.0		0.9		0.9
Disallowed (%)	1.5		0.2		0.0

[a] Values in parentheses correspond to the highest resolution shell (β-SpeC, 3.11–3.00 Å; β-SpeA (apo), 2.9–2.8; β-SpeA (zinc), 2.58–2.49).

[b] $R_{sym} = \Sigma|(I_{hkl} - I_{(hkl)})|/(\Sigma I_{hkl})$, where $I_{(hkl)}$ is the mean intensity of all reflections equivalent to reflection hkl by symmetry.

[c] R_{work} (R_{free}) $= \Sigma||F_o| - |F_c|/\Sigma|F_o||$, where F_c is the calculated structure factor; reflections used in test set include: β-SpeC, 1846 reflections, 4.8%; β-SpeA (apo), 1326 reflections, 4.9%; β-SpeA (zinc), 1871 reflections, 4.8%.

quality. The structure of the complex was solved by molecular replacement using wild-type SpeA [23] and the 14.3.d TCR β chain [25] as search models. Data collection and refinement statistics for both crystal forms are shown in Table 1. Due to the better diffraction and refinement of the zinc-soaked crystals, all subsequent discussion of the β-SpeA complex is limited to this form. Electron density from a composite annealed omit map in the β-SpeA interface is shown in Figure 1C. As in the β-SpeC complex, the SpeA mutation site, C90S, is not involved in TCR β chain, or other crystal contact, interactions. None of the six zinc ions in the zinc-soaked crystals are located in the β-SpeA interface or at the putative MHC class II binding site. A zinc atom is present at the site predicted by Papageorgiou et al. [23], tetrahedrally coordinating SpeA residues Glu33, Asp77, His106, and His110. The physiological role of this site, if any, is unknown.

Multiple Binding Modes for Complexes between Bacterial SAGs and TCR β Chains

The overall structures of the β-SpeC and β-SpeA complexes (Figures 1B and 1D) show, as for the β-SEC3 [18] and β-SEB [19] complexes, that residues in the cleft between the large and small domains of both SAGs make intermolecular contacts with residues from both the CDR loops and FRs of their respective TCR β chain ligands. It is evident, though, that the β-SpeC complex involves a significantly larger number of interface residues than does the β-SpeA complex. Superposition of the TCR β chains of the β-SpeC, β-SpeA, and β-SEB complex structures (Figure 2) reveals that SpeC interacts with its TCR β ligand through an altered orientation relative to that used by SpeA or SEB. SpeC binds in a more encompassing manner to the Vβ domain than do SpeA (Figure 2A) and SEB (Figure 2B). Thus, while portions of the main chain superimpose well at the top
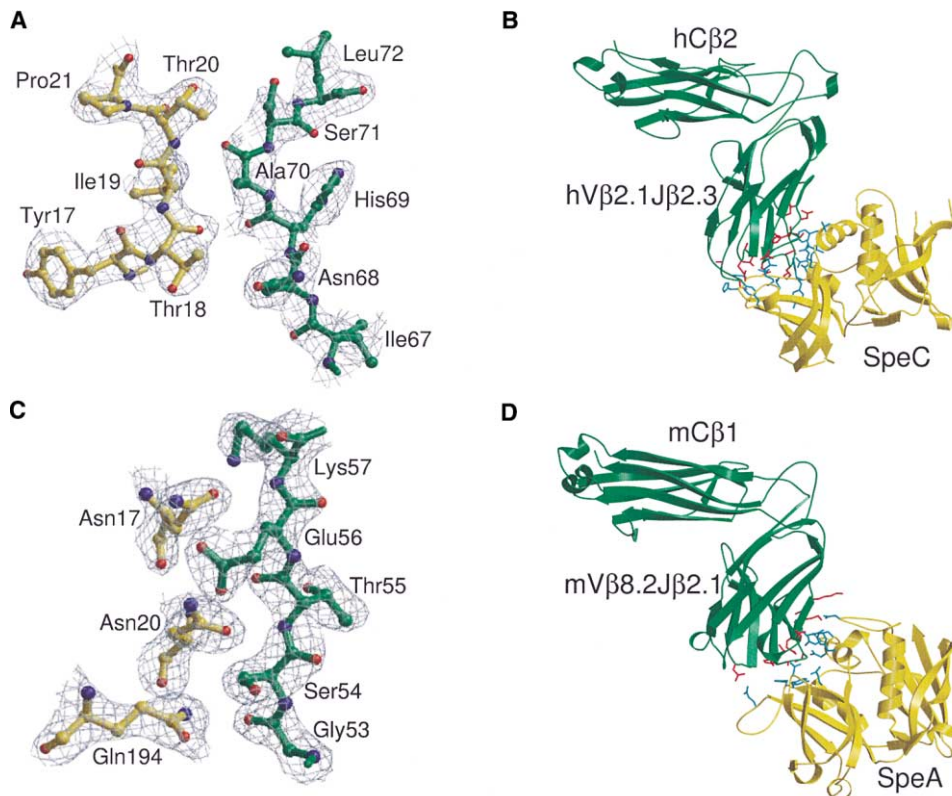
Figure 1. Structural Overview of the SpeC-hVβ2.1 and SpeA-mVβ8.2 Complexes

Final composite annealed omit electron density maps for part of the interface regions of (A) the SpeC-hVβ2.1 complex and (C) the SpeA-mVβ8.2 complex, contoured at 1.5 σ. Structural overviews of (B) the SpeC-hVβ2.1 complex and (D) the SpeA-mVβ8.2 complex. Colors are as follows for both complexes: SAG, yellow; TCR β chain, green; SAG interface residues, cyan; TCR β interface residues, red. Carbon atoms are in yellow for the SAGs and in green for the TCR β chains. Nitrogen atoms, blue; oxygen atoms, red.

end of the interface along the side of the Vβ domain, comprised mainly of FR residues for all of the complex structures, SpeC extends around the apical region of the Vβ domain, comprised predominantly of CDR loops. SpeA and SEB, conversely, bind mVβ8.2 in an essentially analogous orientation (Figure 2C), with contacts restricted largely to the side of the Vβ domain.

The solvent-excluded surface areas of the β-SpeC, β-SpeA, and β-SEB complexes are 1818, 1324, and 1268 Å^2, respectively. The β-SpeA and β-SEB buried surface areas fall within the range observed for antigen-antibody complexes [26] but short of values defined for TCR-peptide/MHC complexes [20, 21, 27, 28]. The β-SpeC complex, however, has a significantly larger buried surface, which is comparable to those of TCR-peptide/MHC complexes.
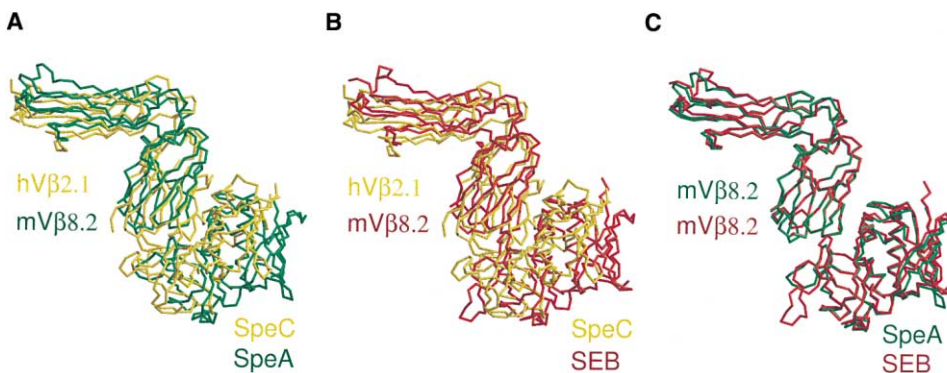

Figure 2. SpeC Adopts a More Apical Position for Its Interaction with Its TCR β Chain Ligand Than Do Other Bacterial Superantigens

Superpositions of (A) the SpeA-mVβ8.2 (green) and SpeC-hVβ2.1 (yellow) complexes, (B) the SpeC-hVβ2.1 (yellow) and SEB-mVβ8.2 (red) complexes, and (C) the SpeA-mVβ8.2 (green) and SEB-mVβ8.2 (red) complexes.
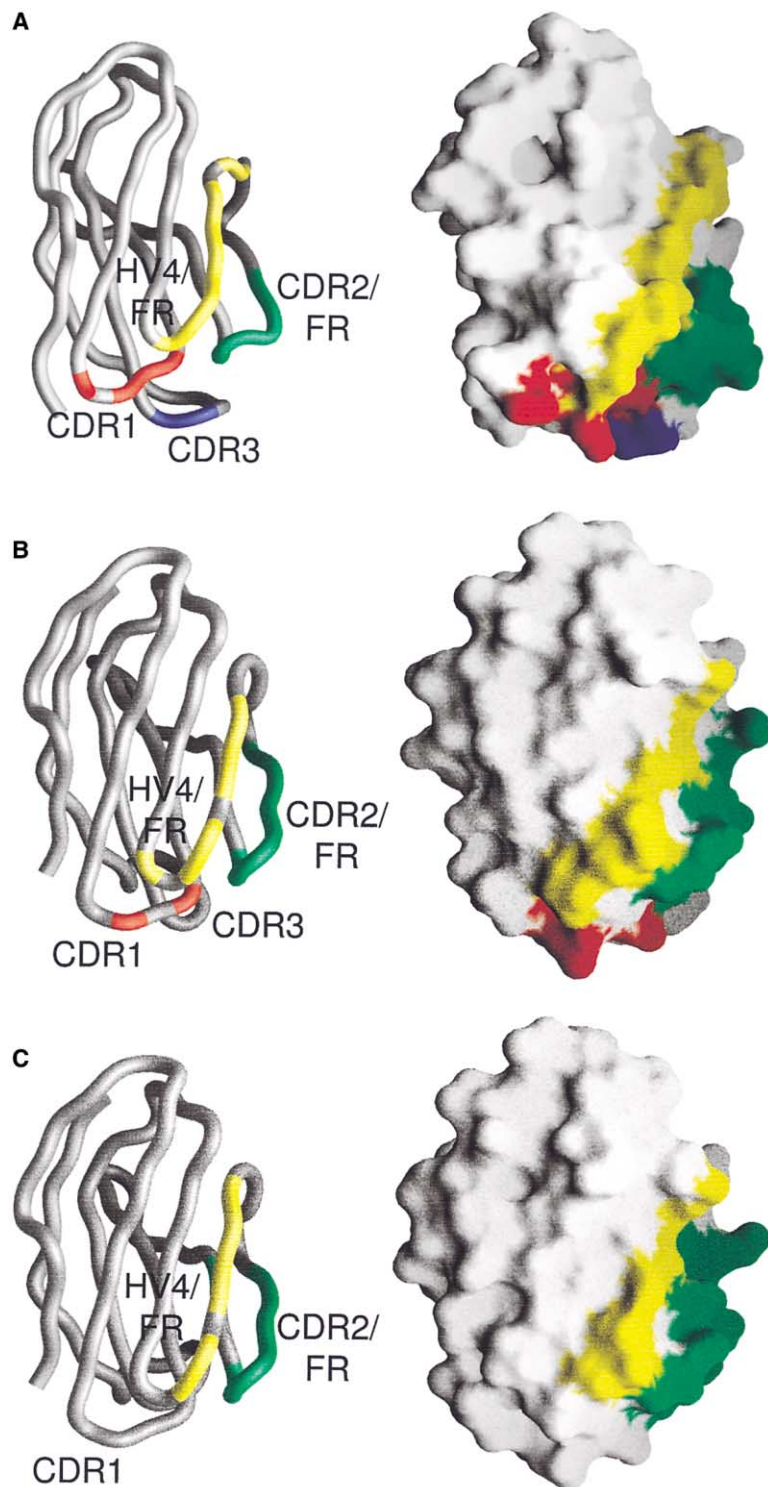
Figure 3. Diverse TCR β Chain Molecular Surface Burial by Bacterial Superantigens

Molecular surface of (A) hVβ2.1 buried by SpeC, (B) mVβ8.2 buried by SpeA, and (C) mVβ8.2 buried by SEB. Colors are as follows: CDR1 buried molecular surface, red; CDR2 and associated FR buried molecular surface, green; HV4 and associated FR buried molecular surface, yellow; CDR3 buried molecular surface, blue.

As shown in Figure 3, there exists not only a quantitative difference in the TCR β chain surface burial by these three SAGs but also a number of qualitative distinctions. SpeC contacts portions of the molecular surface of the hVβ2.1 domain that have previously been shown to be involved in the interface of other SAG-TCR β chain complexes, including residues from CDR2, HV4, FR2, and FR3 (Figures 3A and 3C). Surprisingly, SpeC was also found to contact residues from the CDR1 and CDR3 loops. Together, the hVβ2.1 residues buried by SpeC upon complex formation comprise a large and contiguous molecular surface that extends from more than halfway up the side of the Vβ domain to the extreme bottom of the molecule. While the differences between the pat-

terns of Vβ molecular surface buried by SpeA and SEB (Figures 3B and 3C) are less extensive than between SpeC and SEB, there are some notable differences in their binding modes. SpeA binding to mVβ8.2 results in an extension of the molecular surface buried by SEB to more apical regions of HV4 as well as to CDR1. There are no significant differences in the structures of the Vβ domain bound by SpeA and SEB, except in the CDR3 loop. This region of the TCR β chain, however, makes contacts neither with SpeA nor SEB. Conversely, the TCR β chain ligand of SpeC is structurally distinct from that bound by SpeA and SEB, particularly in its CDRs (see below). The extended conformation of hVβ2.1 CDR3, which points directly toward the interface, contributes at least partially to its involvement in SpeC binding. Notwithstanding differences in Vβ CDRs, there is a significantly higher degree of envelopment of the hVβ2.1 surface by SpeC than by SpeA and SEB of mVβ8.2, likely due to a somewhat deeper and broader cleft between the large and small domains in SpeC compared to those in SpeA and SEB (Figures 1 and 2). Subsequently, the β-SpeC interface is characterized by a large number of contacts involving all three mVβ2.1 CDR loops, HV4, and associated FRs. These contacts are made to atoms in CDR1 (19%), FR2 (3%), CDR2 (34%), FR3 (22%), HV4 (13%), and CDR3 (9%). For the β-SpeA complex, by comparison, the CDR1, CDR2, FR3, and HV4 regions account for 6%, 33%, 50%, and 11%, respectively, of the total contacts to the SAG.

Unlike in the β-SEB complex (Figure 4, right column), where hydrogen bonds are made between SEB side chain and TCR β main chain atoms [19], SpeC forms numerous specific hydrogen bonds and van der Waals interactions with both main chain and side chain atoms of hVβ2.1 (Figure 4, left column). CDR1 residues Gln28, Ala29, and Thr30 contact two discontinuous sets of residues from SpeC, Leu78/Asn79 and Arg45/Tyr49, through a combination of van der Waals contacts and hydrogen bonds. Specific hydrogen bonds between side chains from each molecule in the β-SpeC complex are also observed in the CDR2 portion of the interface. The Oγ atom of Ser52a is sandwiched, through hydrogen bonds, by the side chains of SpeC residues Tyr15 and Arg181, which are also responsible for other hydrogen bonds in this region of the interface. Two hydrogen bonds involving only main chain atoms are observed between His69 and Thr18 of hVβ2.1 and between Ala70 and Thr20 of SpeC. The remainder of the interactions between SpeC and the CDR2 portion of hVβ2.1 is comprised of van der Waals interactions. Interactions in the HV4/FR3 region of hVβ2.1 are similar in nature to those in the β-SEB complex in that they are predominantly comprised of van der Waals interactions and hydrogen bonds to main chain atoms, although they are much more numerous in the former. The long, protruding CDR3 loop of hVβ2.1 points directly toward the SAG, contacting SpeC Asn79 and producing several hydrogen bonds.

While SpeA and SEB interactions with mVβ8.2 have a high degree of similarity, there are a number of distinctive features of their respective interfaces (Figure 4, middle and right columns). Most notable is the hydrogen bond formed between the side chains of Asn28 of the CDR1 loop of mVβ8.2 and Glu94 of SpeA. Glu94 resides in the disulfide loop of SpeA, the region of the two SAGs that diverges the most structurally, due primarily to the difference in length between this loop in SpeA and SEB (10 and 19 residues, respectively). Glu94 and its counterpart in SEB, Thr107, however, are positionally equivalent when the Vβ domains of the β-SpeA and β-SEB complexes are superimposed. Because the position and conformation of the mVβ8.2 CDR1 loop is unchanged between the two complexes, the hydrogen bond, which is formed by SpeA Glu94 and not by SEB Thr107, is simply a result of the length of the side chain at this position in the two SAGs, as both glutamic acid and threonine residues have terminal oxygen atoms with hydrogen bonding capabilities. The interfaces of SpeA and SEB in complex with the CDR2/FR3 region of mVβ8.2 are distinguished primarily by the quantity and quality of hydrogen bonds observed. SEB forms numerous van der Waals interactions but only three hydrogen bonds, all between SEB side chain and mVβ8.2 main chain atoms. In the β-SpeA complex, there exists a similar number of van der Waals contacts, and the three hydrogen bonds observed in the β-SEB complex are retained by analogous residues in the β-SpeA complex. Five additional hydrogen bonds, several of which involve mVβ8.2 side chain atoms, however, are observed in the β-SpeA complex. Interactions in the HV4/FR3 portion of the interfaces of the β-SpeA and β-SEB complexes are nearly identical.

Comparison of MHC Class II-Dependent T Cell Signaling Complexes

A model of the MHC-SEB-TCR ternary complex has been constructed by superposition of the common elements of the SEB-peptide/HLA-DR1 complex [11], the 14.3.d TCR β chain-SEB complex [19], and the 2C αβ TCR heterodimer [29]. In this model (Figure 5B), SEB acts as a wedge, essentially rotating the TCR about a contact point between the MHC α subunit α helix and the TCR β chain CDR2 loop, relative to the HA 306–318 peptide/HLA-DR1-HA1.7 TCR complex [21] (Figure 5A). This effectively prevents the peptide and all of the CDR loops, except Vα CDR2, from making specific contacts in the signaling complex. The interaction between residues from the MHC β chain and the Vα CDR2 loop has been confirmed by biochemical and mutational studies [30] in which positive binding cooperativity was observed when a ternary complex was formed between HLA-DR1, SEC3, and the 14.3.d TCR αβ heterodimer but was absent when a similar complex was formed using only the 14.3.d TCR β chain. It is likely that SpeA crosslinks TCR and MHC in a manner analogous to SEB or SEC3, since SpeA probably binds MHC class II at the same low-affinity site as SEB [23], and, as discussed above, the two toxins have very similar TCR binding sites.

Although no MHC-SpeC-TCR ternary complex structure exists, the SpeC-TCR β chain complex presented here allows us to propose a structural model for the MHC-SpeC-TCR ternary signaling complex, revealing that the crosslinking mechanism utilized by SpeC is completely dissimilar to that of SEB. A model of the MHC-SpeC-TCR ternary signaling complex produced

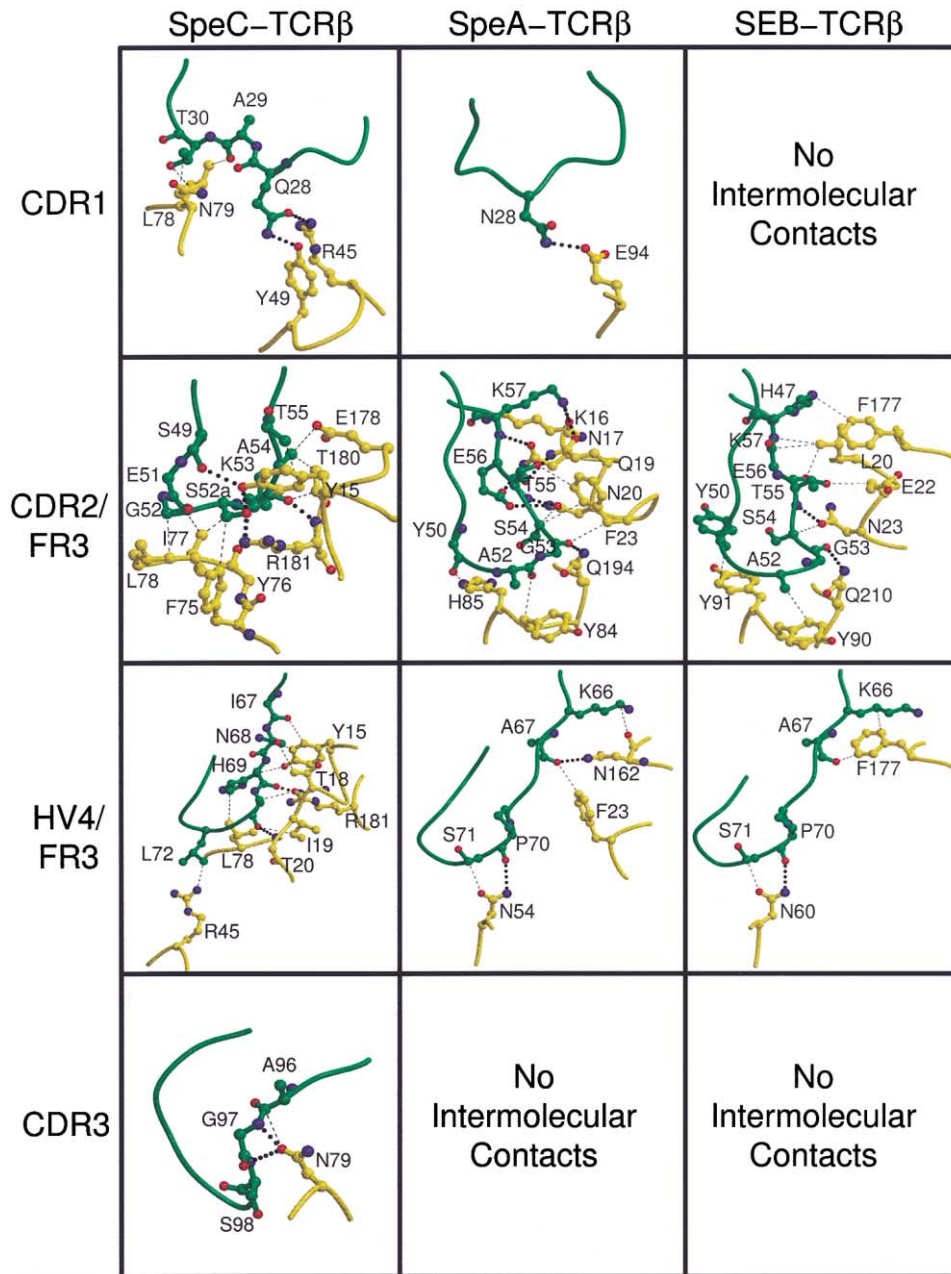|	SpeC–TCRβ	SpeA–TCRβ	SEB–TCRβ
CDR1	A29 T30 Q28 L78 N79 R45 Y49	N28 E94	No Intermolecular Contacts
CDR2/ FR3	S49 T55 E178 A54 K53 T180 E51 S52a Y15 G52 I77 R181 L78 Y76 F75	K57 K16 N17 E56 Q19 T55 N20 Y50 S54 F23 A52 G53 Q194 H85 Y84	H47 F177 K57 L20 E56 E22 Y50 T55 N23 S54 G53 A52 Q210 Y91 Y90
HV4/ FR3	I67 N68 Y15 H69 T18 R181 I19 L72 L78 T20 R45	K66 A67 N162 F23 S71 P70 N54	K66 A67 F177 S71 P70 N60
CDR3	A96 G97 N79 S98	No Intermolecular Contacts	No Intermolecular Contacts

Figure 4. Intermolecular Contacts Resulting from Complexes of SpeC, SpeA, and SEB with Their Respective TCR β Chain Ligands

Intermolecular contacts made in the SpeC-hVβ2.1 complex (left column), the SpeA-mVβ8.2 complex (middle column), and the SEB-mVβ8.2 complex (right column). Contacts are further divided according to those made by the CDR1 loop, CDR2 loop and associated FR residues, HV4 loop and associated FR residues, and CDR3 loop (from top to bottom, respectively). SAG molecule, yellow; TCR β chain, green. Hydrogen bonds are represented by dotted lines, and van der Waals interactions are represented by dashed lines. Main chain and side chain atoms not involved in intermolecular contacts have been omitted for clarity.

by superposition of the common elements of the SpeC-MBP 89–101 peptide/HLA-DR2a complex [13], the β-SpeC complex presented in this study, and the 2C αβ TCR heterodimer [29] is shown in two orientations in Figures 5C and 5D. Unlike the MHC-TCR crosslinking mechanism of SEB, SpeC acts as a bridge between the MHC and TCR molecules. This results in a displacement of the TCR away from its position in the MHC-TCR complex (Figure 5A) and a complete disruption of any possi-ble MHC-TCR contacts. When the MHC-SpeC-TCR model is viewed in the two orientations shown (Figures 5C and 5D), it is apparent that the TCR in the MHC-SpeC-TCR model is rotated, relative to the MHC-TCR complex, about the horizontal axis by a similar amount to that in the MHC-SEB-TCR model, but in the opposite direction, and about the vertical axis by approximately 90°. As for the MHC-TCR complex and the MHC-SEB-TCR model, the carboxyl termini of the MHC and TCR
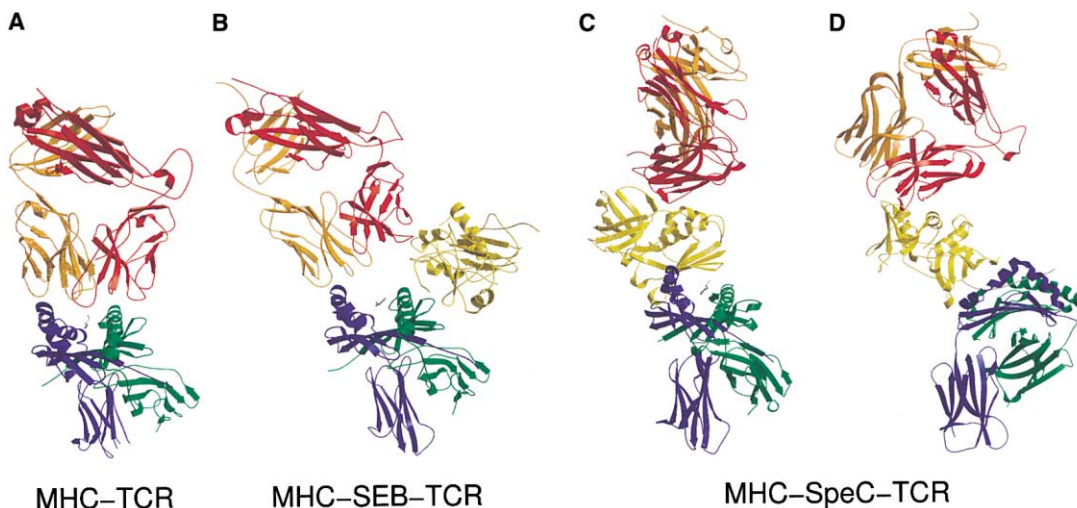
Figure 5. Comparison of MHC Class II-Dependent T Cell Signaling Complexes

(A) The TCR-peptide/MHC complex [21].

(B) A model of the MHC-SEB-TCR ternary complex, produced by superposition of the common elements of the SEB-peptide/HLA-DR1 [11], 14.3.d TCR β chain-SEB [19], and the 2C αβ TCR complexes [29].

(C and D) Two views of the MHC-SpeC-TCR ternary complex model produced by the superposition of the SpeC-MBP 89–101 peptide/HLA-DR2a complex [13], the β-SpeC complex presented in this study, and the 2C αβ TCR complex [29]. In the first view (C), the MHC molecule is approximately aligned with that in the MHC-TCR (A) and MHC-SEB-TCR (B) complexes. The second view of the MHC-SpeC-TCR complex (D) is rotated by approximately 90° about the vertical axis. In all panels, the colors are as follows: MHC α chain, green; MHC β chain, blue; antigenic peptide, gray; TCR α chain, orange; TCR β chain, red; SAG, yellow.

α and β chains (which enter their respective cell membranes) in the MHC-SpeC-TCR model are aligned such that this ternary signaling complex could easily be accommodated between two interacting cells. Although the MHC-SpeC-TCR ternary complex is slightly extended compared to the MHC-SEB-TCR complex, this increase in intermembrane length is small compared to those that have been found to affect the conservation of distance within the immunological synapse to such an extent that T cell activation is disrupted [31].

Discussion

Previous crystal structures of SAG-TCR β chain complexes [18, 19] have revealed only a single binding mode for these types of interactions. Both SEC3 and SEB bind to mVβ8.2 predominantly through contacts with residues from CDR2, HV4, and their associated FRs. Furthermore, all of the hydrogen bonds in these complexes involve only main chain atoms of mVβ8.2, and, thus, it has been proposed that their binding mechanism is one of simple conformational dependence [18, 19]. We define conformationally dependent binding as interactions that rely predominantly on the protein backbone atomic structure of the Vβ domain, largely independent of amino acid sequence, and, consequently, of side chain structure. Structural variation in Vβ domains is mainly restricted to its three CDR loops extending from a common structural foundation, the framework region. Even the first two CDR loops, however, are not excessively variable. A recent analysis of Vβ gene segments and known atomic structures [32] estimates that 90 percent of these gene segments have CDR1 and CDR2 loops of any of three known canonical structures each.

CDR3 loops of TCR β chains are much more variable in sequence and structure due the recombination of Vβ-Dβ-Jβ gene segments. Thus, SAGs such as SEC3 and SEB that depend only on the backbone conformation of one of the relatively invariable CDR loops will not have a high Vβ domain binding specificity.

Clearly, the small sample size of available SAG-TCR β complexes has hampered a comprehensive analysis of these interactions. The structures presented here, including SpeA complexed with the same 14.3.d TCR β chain that has been used previously in SAG-TCR structural studies as well as SpeC complexed with a human TCR β chain that has never before been characterized structurally, expand the available database of complex structures significantly, demonstrate that there exist multiple binding modes for SAG-TCR interactions, and help to elucidate the structural basis for Vβ specificity by SAGs.

Relative to other SAGs, SpeC binds TCR β chains in a highly specific manner, primarily activating human T cells bearing Vβ2.1 [33]. While the β-stranded core of the hVβ2.1 domain is very similar to that of mVβ8.2, the binding surface of hVβ2.1 presented to SpeC differs significantly from that of the SpeA- and SEB-specific mVβ8.2 and is unique in relation to the structures of other Vβ domains. Several features of hVβ2.1 contribute clearly to its specificity for SpeC. These include two single amino acid insertions, one each in CDR1 and CDR2, and an extended CDR3 loop.

The CDR1 insert (Phe27a) results in a semi-rigid-body movement of this loop away from its position in other Vβ domains and toward the SpeC molecule in the β-SpeC structure. The consequence of this CDR1 rearrangement is an average displacement of hVβ2.1 residues Gln28,

Ala29, and Thr30 by 1.7 Å closer to SpeC, relative to the positions of analogous residues of mVβ8.2 CDR1 in the β-SpeA complex. Without such a movement, the numerous hydrogen bonds and van der Waals interactions between SpeC and these three hVβ2.1 residues could not be formed.

The CDR2 loop of hVβ2.1 possesses two noteworthy structural features. First, it has a single residue insert, relative to other Vβ domains, common only to hVβ2.1 and hVβ4.1 and their mouse analogs, mVβ15.1 and mVβ18.1 [34]. Additionally, this CDR2 loop has been predicted to have a noncanonical conformation [32], a feature that is apparent in Figure 4, in relation to the CDR2 loop of mVβ8.2. That the inserted residue in CDR2, Ser52a, appears to be responsible for the most productive interactions in the β-SpeC complex is not surprising, considering that SpeC is highly specific for Vβ domains that share these rare CDR2 features [33]. The recent development of SpeC vaccine toxoids that protected rabbits from streptococcal toxic shock syndrome included mutation of Tyr15 to alanine [35], which presumably abolishes their T cell stimulating capacities, indirectly supporting the energetic importance of the electrostatic interactions formed between SpeC and Ser52a of hVβ2.1. It is interesting to note that, while SpeC interacts with both hVβ2.1 and hVβ4.1, stimulation of human T cells bearing Vβ2.1 is 15-fold greater than those presenting Vβ4.1 domains [33]. The sequence of hVβ4.1 includes the Ser52a-inserted residue in its CDR2 loop but lacks the hVβ2.1-like insertion in CDR1. Other Vβ domains that have the CDR1 insertion but lack the one in CDR2, such as hVβ20.1, are not recognized by SpeC. Thus, of these two rare insertions, the CDR2 insertion may confer SAG binding specificity, while the CDR1 insertion may be responsible for increased affinity.

The extended conformation of the hVβ2.1 CDR3 loop results in several specific intermolecular contacts with SpeC (Figures 3A and 4). The hVβ2.1 CDR3 residues in contact with SpeC derive from Vβ-Dβ-Jβ recombination and, thus, are not present in all human Vβ domains. As no structure of this TCR β chain exists in its uncomplexed form, it is impossible to determine whether this is simply a serendipitous interaction due to the flexibility of the CDR3 loop. Indeed, a model of a complex between SEB and hVβ12.3 [2, 27] shows that CDR3 Leu98, also derived from Vβ-Dβ-Jβ recombination, would be positioned close enough to SEB to form specific contacts. In the β-SpeA and β-SEB complexes, the identical mVβ8.2 CDR3 loop has markedly different conformations (Figures 3B and 3C). Furthermore, flexibility of TCR CDR3 loops is not uncommon and has been proposed to be important in TCR recognition of peptide/MHC complexes [28]. It may be that protein plasticity in the Vβ domain is also important in SAG recognition. While the β-SpeC complex described here represents the first structural example of CDR3 involvement in SAG binding, Vβ CDR3 residues have been reported to influence T cell reactivity toward other microbial SAGs, namely *Mycoplasma arthritidis* mitogen (MAM) [36] and mouse retroviral Mtv-9 SAG (vSAG9) [37]. Although this precludes the β-SpeA or β-SEB binding mode for MAM and vSAG9 interactions with their respective TCR β chain ligands, there also exists no evidence that these SAGs utilize the

β-SpeC binding mode, and they may thus form further distinct complexes with TCR.

While there is some overlap in Vβ binding specificity between SpeA and SEB, namely mVβ8.2 and the homologous hVβ12.2 and hVβ14.1 [38, 39], SpeA is a much more specific stimulator of T cells than SEB, which also recognizes mVβ3, 7, 10, 11, and 17 and hVβ3, 5, 12, 13, 14, 15, 17, and 20 [2, 17]. At least part of the reason for this striking difference in Vβ specificity can be deduced from the β-SEB and β-SpeA complex structures. In the former complex, all the hydrogen bonds between SEB and Vβ are formed between SEB side chain atoms and Vβ main chain atoms, such that SEB is able to bind a variety of Vβ domains whose corresponding main chain atoms are at positions similar to those in mVβ8.2, largely independent of side chains [19]. In the β-SpeA complex, by contrast, the majority of interface hydrogen bonds involve side chain atoms from either, or both, the SAG and Vβ molecules, including a greater overall number of hydrogen bonds (Figure 4, middle and right columns). Thus, SpeA seems to require some Vβ sequence specificity that restricts its reactivity beyond the simple conformation dependence required by SEB. The increased number of intermolecular interactions in the β-SpeA complex versus the β-SEB complex may also explain the difference in affinity of these two SAGs for the common mVβ8.2 target, with which SpeA forms an approximately 20-fold tighter complex than SEB [24]. Alternatively, the higher affinity of SpeA for mVβ8.2 may derive, at least in part, from its interaction with the CDR1 loop.

Interestingly, SpeA also stimulates human T cells bearing Vβ2.1 domains [38, 39]. It is unlikely that SpeA binds hVβ2.1 in a manner analogous to SpeC, as none of the SpeC residues identified in the interface with this Vβ are conserved in SpeA. It may be even less likely that SpeA binding to hVβ2.1 involves the same binding mode observed in its complex with mVβ8.2. First, much of the Vβ domain surface that forms the interface with SpeA in mVβ8.2 is dramatically altered in hVβ2.1, largely due to the two amino acid insertions in CDR1 and CDR2 discussed above. Second, when recombinant wild-type SpeA and a panel of mutants were tested for the ability to stimulate hVβ2.1-positive T cells [39], there was no correlation between the effect of specific mutations and the SpeA residues that we have shown here to be involved in binding mVβ8.2. Thus, it is most probable that the SpeA-hVβ2.1 complex will provide a binding mode distinct from that seen for the SpeA-mVβ8.2 or SpeC-hVβ2.1 interactions. Human Vβ2.1 is also the exclusive target of TSST-1 [4]. Like SpeA, TSST-1 shares little sequence homology with SpeC, and its as yet undetermined complex with hVβ2.1 may represent still another SAG binding mode to this Vβ domain.

With this more diverse range of SAG-TCR interactions now characterized on the structural level, we can begin to observe a new paradigm for the selectivity of T cell activation by SAGs, depending on varying levels of Vβ domain specificity. One group of highly promiscuous T cell activators, including SEB and SEC3, binds TCR β chains in the simple conformation-dependent manner described above and interacts with only a single CDR loop, CDR2. Moderately promiscuous T cell activators, including SpeA, can be grouped together on the basis

of their dependence on numerous specific interactions mediated by direct side chain to side chain contacts overlayed onto the conformation dependence of the first group and the additional involvement of the CDR1 loop. A third group of highly selective T cell activators, including SpeC, binds those TCR Vβ domains that have the highest degree of structural dissimilarity, including non-canonical CDR loop conformations and residue insertions as well as usage of all three CDR loops, incorporating the highly variable CDR3 loop. TSST-1, which activates only human T cells bearing Vβ2.1 domains, may be the most extreme example in this third selectivity group.

Even though TCR is engaged very differently in TCR-MHC, TCR-SEB/SEC-MHC, and TCR-SpeC-MHC complexes, it is remarkable that the end result—highly efficient T cell activation—is very similar. This strongly implies that the specific geometry of TCR ligation may be less critical than other factors, such as the affinity and kinetics of the binding reaction, in triggering T cells. Indeed, we have previously shown that the half-life of the TCR-SEC3-MHC complex (∼8 s) [30] falls within the range measured for specific TCR-peptide/MHC complexes (1–60 s) [40]. In this case, maximum stabilization is achieved through direct TCR-MHC interactions that compensate for the weak individual affinities of SEC3 for TCR and MHC and increase the overall half-life of the ternary signaling complex. Although we have not measured the half-life of the TCR-SpeC-MHC complex, we expect that it, too, will be comparable to those of TCR-peptide/MHC complexes. However, since direct TCR-MHC interactions are precluded in the TCR-SpeC-MHC complex, sufficient stabilization must be achieved through the interplay of TCR-SAG and SAG-MHC interactions alone. This suggests that the far higher affinity of the SpeC-MHC relative to the SEC3-MHC interaction ($K_DS \approx 4 \times 10^{-8}$ M and 3×10^{-4} M, respectively) [13, 30] may circumvent the need for TCR-MHC contacts in the TCR-SpeC-MHC complex.

Biological Implications

Superantigens are potent immunomodulators, eliciting massive T cell proliferation through simultaneous interaction with MHC class II and TCR molecules. This can result in the release of inordinate quantities of pyrogenic and inflammatory cytokines, leading to disease. Determining the structural basis for the T cell stimulatory capabilities of SAGs is a key step in understanding SAG-induced disease pathogenesis and the possible development of effective therapeutics, a task that is made difficult due to the variability in the binding modes of the SAG to both its MHC and TCR binding partners. While this binding variability has been well defined crystallographically for SAG-MHC complexes, interaction variability and, subsequently, TCR Vβ domain specificity in SAG-TCR complexes have not been nearly as well elucidated on the structural level. The SAG-TCR β chain structures presented in this study have significantly increased our understanding of the structural basis for T cell activation by SAGs. These structures show why certain SAGs bind to a wide range of TCR Vβ domains

and stimulate a very large fraction of all T cells, while others are much more restricted in TCR binding and T cell activation. Although the number of SAG-TCR complex structures is still quite low, the limited available database has allowed the identification of some correlations between the Vβ domain specificity of SAGs and certain structural characteristics of the Vβ domain hypervariable regions that they bind. Currently, the structures of two SAGs, SEB and SpeC, have been determined in complex with both of their respective MHC and TCR binding partners, allowing comparison of structural models of the SEB- and SpeC-dependent MHC-SAG-TCR complexes. The MHC-SEB-TCR signaling complex is dependent on low-affinity interactions between SAG-MHC and SAG-TCR as well as a direct MHC-TCR interface. This results in overall ternary complex stability that is similar to those for peptide/MHC-TCR complexes. SpeC abrogates all direct contacts between MHC and TCR molecules in the MHC-SpeC-TCR complex, whose stability relies on a high-affinity interaction between SpeC and MHC and a low-affinity interaction between SpeC and TCR. While SEB and SpeC produce significantly different ternary T cell signaling complexes in terms of their molecular architectures, they nevertheless result in very similar T cell responses.

Experimental Procedures

Protein Expression and Purification
Soluble, unglycosylated 14.3.d TCR β chain (mVβ8.2) was produced as described previously [18]. The SpeA(C90S) and SpeC(H35A) mutants were expressed in *Escherichia coli* BL21(DE3) as described [35]. The SAGs were purified by successive preparative flatbed iso-electric focusing, using pH gradients of 3.5–10 and 6–8. SpeA(C90S) was further purified by ion exchange chromatography using a MonoQ anion exchange column (Pharmacia) equilibrated with 20 mM Tris-HCl (pH 8.5) developed with a linear NaCl gradient. Further purification of SpeC(H35A) was carried out by size exclusion chromatography on a Superdex 75 FPLC column (Pharmacia) equilibrated with HBS. The gene encoding human Vβ2.1Dβ2.1Jβ2.3Cβ2, kindly provided by U. Utz and R.-P. Sékaly (University of Montreal), was cloned between the NdeI and EcoRI restriction sites of the pET17b expression vector (Novagen). Residues Cys13 and Cys191 of the mature protein were mutated to Ala using the Quik Change Mutagenesis Kit (Stratagene). Expression of hVβ2.1 was carried out in *E. coli* BL21(RIL), and protein from inclusion body preparations was folded in vitro in 100 mM Tris-HCl (pH 8.5), 900 mM arginine-HCl, 100 mM L-arginine, 2 mM EDTA, 6.3 mM cysteamine, and 3.7 mM cystamine. Properly folded material was purified in two steps, first by size exclusion chromatography using a Superdex 75 column equilibrated in 25 mM Tris-HCl (pH 7.5) and 150 mM NaCl and subsequently by anion exchange chromatography using a MonoQ column equilibrated in 20 mM Tris-HCl (pH 8.5) developed using a linear NaCl gradient.

Crystallization and Data Collection
Crystals of the SpeA(C90S)-mVβ8.2 complex were grown at room temperature in hanging drops by mixing 1 μl of complex solution (containing an equimolar ratio of mVβ8.2 and SpeA(C90S) at a total protein concentration of 8 mg/mL) with an equal volume of reservoir solution containing 15% polyethylene glycol (PEG) 8000, 0.2 M MgCl₂, and 0.1 M Tris-HCl (pH 8.0). Crystals were washed three times with mother liquor and transferred to a cryoprotectant solution (mother liquor containing 25% glycerol) prior to flash cooling in liquid propane. Crystals in the presence of zinc were prepared by soaking the native crystals in 5 mM ZnCl₂ for 6 hr prior to flash cooling. X-ray diffraction data were collected on an ADSC Quantum-4 CCD detector from a single complex crystal at 100 K on beamline 19-ID (λ = 0.978 Å) of Argonne National Laboratory. The SpeA(C90S)-

mVβ8.2 complex crystallized in space group P2₁ with cell dimensions $a = 71.4$ Å, $b = 83.3$ Å, $c = 93.6$ Å, and $\beta = 91.6°$ and diffracted to a nominal resolution of 2.8 Å. The zinc-soaked crystals were essentially isomorphous, with cell dimensions $a = 71.7$ Å, $b = 83.7$ Å, $c = 93.9$ Å, and $\beta = 91.7°$, but diffracted to 2.5 Å resolution. Diffraction data were processed and scaled using HKL2000/SCALEPACK [41], and data reduction was completed using programs from the CCP4 suite [42].

Crystals of SpeC(H35A)-hVβ2.1 were grown at room temperature in hanging drops by mixing 1 μl of complex solution (containing an equimolar ratio of SpeC(H35A) and TCR β chain at a total protein concentration of 10 mg/ml) with an equal volume of reservoir solution containing 5% PEG 6000, 0.1 M LiCl, and 0.1 M HEPES (pH 7.0). Crystals were washed prior to transfer to cryoprotectant solution (mother liquor containing 20% ethylene glycol) and flash cooling in liquid propane. Diffraction data were collected on an ADSC Quantum-4 CCD detector on beamline F-1 ($\lambda = 0.943$) at the Cornell High Energy Synchrotron Source. The SpeC(H35A)-hVβ2.1 complex crystallized in space group P2₁ with cell dimensions of $a = 57.4$ Å, $b = 146.9$ Å, $c = 136.0$ Å, and $\beta = 98.7°$ and diffracted to a nominal resolution of 3.0 Å. Diffraction data were processed and scaled using DENZO and SCALEPACK [41], and data reduction was completed using programs from the CCP4 suite [42]. Data collection statistics for all of the complex structures are shown in Table 1.

Structure Determination and Refinement

The structure of the zinc-soaked SpeA(C90S)-mVβ8.2 complex was solved by molecular replacement methods using the program AMoRe [43], with crystal structures of SpeA (PDB ID code 1B1Z) and the 14.3.d TCR β chain (PDB ID code 1BEC) as search models. The solution for SpeA was found first, and its position was fixed in order to locate the TCR β chain with the phased translation function calculation. The initial model solutions gave a correlation coefficient of 64.5% and an R factor of 40.3% at a resolution range of 10–4 Å. Refinement was carried out using CNS [44], including rigid-body refinement, iterative cycles of simulated annealing, positional refinement, torsion angle refinement, and temperature factor (B) refinement, interspersed with model rebuilding into σ_A-weighted $F_o - F_c$ and $2F_o - F_c$ electron density maps using TURBO-FRODO [45]. Water molecules were added only to ($F_o - F_c$) density higher than 3 σ and standard hydrogen bonding geometry. In the final model, six zinc ions and one glycerol molecule were identified. The partially refined structure of the zinc-soaked SpeA-mVβ8.2 complex was used as a starting model for the apo form. Structure refinement for the apo complex progressed similarly to the zinc-soaked form from this point, as described above.

Determination of the SpeC(H35A)-hVβ2.1 complex structure was carried out by molecular replacement with AMoRe [43]. Using the crystal structure of SpeC (Protein Data Bank ID code 1AN8) as a model, four SpeC molecules were placed in the asymmetric unit. Each additional SpeC monomer solution resulted in a higher correlation coefficient and lower R factor than the previous solution. The solution for the four SpeC molecules in the asymmetric unit resulted in a correlation coefficient of 43.3% and an R factor of 43.1% in the resolution range of 8–3.5 Å. Extensive attempts to locate the hVβ2.1 molecules by molecular replacement were made using models of all of the TCR β chains currently in the database in various forms (i.e., wild-type, polyalanine, and loop-truncated models). No TCR β molecular replacement solutions resulted in increased correlation coefficient and decreased R factor, and no solutions resulted in acceptable molecular packing in the unit cell. Rigid-body refinement of the four SpeC model resulted in an R$_{free}$ of 46.2%. $2F_o - F_c$ electron density maps calculated with phases from the four SpeC molecules and solvent flipping were produced using CNS [44] and revealed density for part of the core β sheet structure of one Vβ immunoglobulin (Ig) domain. Manual fitting of a partial Ig core polyalanine model into this density using XtalView [46] and subsequent rigid-body refinement resulted in a reduced R$_{free}$ of 45.1%. $2F_o - F_c$ density modified maps phased with the new model were produced and revealed density corresponding to previously uninterpretable regions of two hVβ2.1 molecules in the asymmetric unit. Several rounds of density-modified, model-phased electron density map production and manual chain tracing were required to produce a model that included essentially all of one hVβ2.1 molecule, a second Vβ domain, and portions of the core region of the second Cβ Ig domain. Although four structurally equivalent β-SpeC complexes exist in the asymmetric unit, as evidenced by noncrystallographic symmetry, crystal packing constraints, and electron density, manual fitting of any portion of the third or fourth TCR β chains did not improve the overall refinement statistics and were therefore left out of the final model. This also proved to maximize the data to parameters ratio, as inclusion of the poorly defined β chains pushed this ratio to unacceptable levels. Refinement and model building was then carried out in a more conventional manner with iterative cycles of positional, torsion angle, and B factor refinement, interspersed with model rebuilding into σ_A-weighted $F_o - F_c$, $2F_o - F_c$, and composite annealed omit electron density maps using XtalView [46]. Only procedures that minimized R$_{free}$ were followed, and the discrepancy between R$_{free}$ and R$_{cryst}$ was kept as small as possible. Noncrystallographic restraints on the four SpeC molecules were relaxed and eventually eliminated throughout the refinement, concomitant with obvious differences in electron density for multiple regions of the four SpeC molecules and a decrease in R$_{free}$ values. Due to the relatively low resolution of the structure, no water molecules were built into the model. The region of the crystal involved in the interaction between SpeC and the first TCR β chain molecule appears to be the most ordered, as reflected by the lower mean temperature (B) factors (Table 1); disorder increases as the distance from the interface becomes greater, with the second Cβ domain displaying the highest mean B factor. The majority of missing residues in the model are either from chain termini, the poorly ordered second Cβ domain, or the missing third and fourth TCR β chains. Current refinement statistics for all of the complex structures are summarized in Table 1. Figures were produced with Molscript [47], Bobscript [48], Raster3D [49], and GRASP [50].

References

1. Sundberg, E.J., Li, Y., and Mariuzza, R.A. (2002). So many ways of getting in the way: diversity in the molecular architecture of superantigen dependent T cell signaling complexes. Curr. Opin. Immunol. *14*, 36–44.

2. Li, H., Llera, A., Malchiodi, E.L., and Mariuzza, R.A. (1999). The structural basis of T cell activation by superantigens. Annu. Rev. Immunol. *17*, 435–466.

3. Dinges, M.M., Orwin, P.M., and Schlievert, P.M. (2000). Exotoxins of *Staphylococcus aureus*. Clin. Microbiol. Rev. *13*, 16–34.

4. McCormick, J.K., and Schlievert, P.M. (2000). Toxins and superantigens of group A streptococci. In Gram Positive Pathogens, V. Fischetti, R. Novick, J. Ferretti, D. Portnoy, and J. Rood, eds. (Washington, D.C.: American Society for Microbiology), pp. 43–52.

5. Renno, T., and Acha-Orbea, H. (1996). Superantigens in autoimmune disease: still more shades of gray. Immunol. Rev. *154*, 175–191.

6. Dalwadi, H., Wei, B., Kronenberg, M., Sutton, C.L., and Braun, J. (2001). The Crohn's disease-associated bacterial protein I2 is a novel enteric T cell superantigen. Immunity *15*, 149–158.

7. Stauffer, Y., Marguerat, S., Meylan, F., Ucla, C., Sutkowski, N., Huber, B., Pelet, T., and Conrad, B. (2001). Interferon-α induced endogenous superantigen: a model linking environment and autoimmunity. Immunity *15*, 591–601.

8. Lavoie, P.M., Thibodeau, J., Cloutier, I., Busch, R., and Sékaly, R.-P. (1997). Selective binding of bacterial toxins to major histocompatibility complex class II-expressing cells is controlled by invariant chain and HLA-DM. Proc. Natl. Acad. Sci. USA *94*, 6892–6896.

9. Tiedemann, R.E., and Fraser, J.D. (1996). Cross-linking of MHC class II molecules by staphylococcal enterotoxin A is essential for antigen-presenting cell and T cell activation. J. Immunol. *157*, 3958–3966.

10. Roussel, A., Anderson, B.F., Baker, H.M., Fraser, J.D., and Baker, E.N. (1997). Crystal structure of the streptococcal superantigen SPE-C: dimerization and zinc-binding suggest a novel mode of interaction with MHC class II molecules. Nat. Struct. Biol. *4*, 635–643.

11. Jardetzky, T.S., Brown, J.H., Gorga, J.C., Stern, L.J., Urban, R.G., Chi, Y.I., Stauffacher, C., Strominger, J.L., and Wiley, D.C. (1994). Three-dimensional structure of a human major histocompatibility molecule complexed with superantigen. Nature *368*, 711–718.

12. Kim, J., Urban, R.G., Strominger, J.L., and Wiley, D.C. (1994). Toxic shock syndrome toxin-1 complexed with a class II major histocompatibility molecule HLA-DR1. Science *266*, 1870–1874.

13. Li, Y., Li, H., Dimasi, N., McCormick, J.K., Martin, R., Schuck, P., Schlievert, P.M., and Mariuzza, R.A. (2001). Crystal structure of a superantigen bound to the high-affinity, zinc-dependent site on MHC class II. Immunity *14*, 93–104.

14. Petersson, K., Hakansson, M., Nilsson, H., Forsberg, G., Svensson, L.A., Liljas, A., and Walse, B. (2001). Crystal structure of a superantigen bound to MHC class II displays zinc and peptide dependence. EMBO J. *20*, 3306–3312.

15. Abrahmsen, L., Dohlsten, M., Segren, S., Bjork, P., Jonsson, E., and Kalland, T. (1995). Characterization of two distinct MHC class II binding sites in the superantigen staphylococcal enterotoxin A. EMBO J. *14*, 2978–2986.

16. Hudson, K.R., Tiedemann, R.E., Urban, R.G., Lowe, S.C., Strominger, J.L., and Fraser, J.D. (1995). Staphylococcal enterotoxin A has two cooperative binding sites on major histocompatibility complex class II. J. Exp. Med. *182*, 711–720.

17. Scherer, M.T., Ignatowicz, L., Winslow, G.M., Kappler, J.W., and Marrack, P. (1993). Superantigens: bacterial and viral proteins that manipulate the immune system. Annu. Rev. Cell Biol. *9*, 101–128.

18. Fields, B.A., Malchiodi, E.L., Li, H., Ysern, X., Stauffacher, C.V., Schlievert, P.M., Karjalainen, K., and Mariuzza, R.A. (1996). Crystal structure of the β chain of a T-cell receptor complexed with a superantigen. Nature *384*, 188–192.

19. Li, H., Llera, A., Tsuchiya, D., Leder, L., Ysern, X., Schlievert, P.M., Karjalainen, K., and Mariuzza, R.A. (1998). Three-dimensional structure of the complex between a T cell receptor β chain and the superantigen staphylococcal enterotoxin B. Immunity *9*, 807–816.

20. Reinherz, E.L., Tan, K., Tang, L., Kern, P., Liu, J., Xiong, Y., Hussey, R.E., Smolyar, A., Hare, B., Zhang, R., et al. (1999). The crystal structure of a T cell receptor in complex with peptide and MHC class II. Science *286*, 1913–1921.

21. Hennecke, J., Carfi, A., and Wiley, D.C. (2000). Structure of a covalently stabilized complex of a human $\alpha\beta$ T cell receptor, influenza HA peptide and MHC class II molecule, HLA-DR1. EMBO J. *19*, 5611–5624.

22. Leggiadro, R.J., Bugnitz, M.C., Peck, B.A., Luedtke, G.S., Kim, M.H., Kaplan, E.L., and Schlievert, P.M. (1993). Group A streptococcal bacteremia in a mid-south children's hospital. South. Med. J. *86*, 615–618.

23. Papageorgiou, A.C., Collins, C.M., Gutman, D.M., Kline, J.B., O'Brien, S.M., Tranter, H.S., and Acharya, K.R. (1999). Structural basis for the recognition of superantigen streptococcal pyrogenic exotoxin A (SpeA1) by MHC class II molecules and T-cell receptors. EMBO J. *18*, 9–21.

24. Malchiodi, E.L., Eisenstein, E., Fields, B.A., Ohlendorf, D.H., Schlievert, P.M., and Mariuzza, R.A. (1995). Superantigen bind-ing to a T cell receptor of known three-dimensional structure. J. Exp. Med. *182*, 1833–1845.

25. Bentley, G.A., Boulot, G., Karjalainen, K., and Mariuzza, R.A. (1995). Crystal structure of the β chain of a T cell antigen receptor. Science *267*, 1984–1987.

26. Lo Conte, L., Chothia, C., and Janin, J. (1999). The atomic structure of protein-protein recognition sites. J. Mol. Biol. *285*, 2177–2198.

27. Garboczi, D.N., Ghosh, P., Utz, U., Fan, Q.R., Biddison, W.E., and Wiley, D.C. (1996). Structure of the complex between human T-cell receptor, viral peptide and HLA-A2. Nature *384*, 134–141.

28. Garcia, K.C., Degano, M., Pease, L.R., Huang, M., Peterson, P.A., Teyton, L., and Wilson, I.A. (1998). Structural basis of plasticity in T cell receptor recognition of a self peptide-MHC antigen. Science *279*, 1166–1172.

29. Garcia, K.C., Degano, M., Stanfield, R.L., Brunmark, A., Jackson, M.R., Peterson, P.A., Teyton, L., and Wilson, I.A. (1996). An $\alpha\beta$ T cell receptor structure at 2.5 Å and its orientation in the TCR-MHC complex. Science *274*, 209–219.

30. Andersen, P.S., Lavoie, P.M., Sekaly, R.P., Churchill, H., Kranz, D.M., Schlievert, P.M., Karjalainen, K., and Mariuzza, R.A. (1999). Role of the T cell receptor α chain in stabilizing TCR-superantigen-MHC class II complexes. Immunity *10*, 473–483.

31. Wild, M.K., Cambiaggi, A., Brown, M.H., Davies, E.A., Ohno, H., Saito, T., and van der Merwe, P.A. (1999). Dependence of T cell antigen recognition on the dimensions of an accessory receptor-ligand complex. J. Exp. Med. *190*, 31–41.

32. Al-Lazikani, B., Leek, A.M., and Chothia, C. (2000). Canonical structures for the hypervariable regions of T cell $\alpha\beta$ receptors. J. Mol. Biol. *295*, 979–995.

33. Li, P.-L., Tiedemann, R.E., Moffat, S.L., and Fraser, J.D. (1997). The superantigen streptococcal pyrogenic exotoxin C (SPE-C) exhibits a novel mode of action. J. Exp. Med. *186*, 375–383.

34. Rowen, L., Koop, B.F., and Hood, L. (1996). The complete 685-kilobase DNA sequence of the human β T cell receptor locus. Science *272*, 1755–1762.

35. McCormick, J.K., Tripp, T.J., Olmsted, S.B., Matsuka, Y.V., Gahr, P.J., Ohlendorf, D.H., and Schlievert, P.M. (2000). Development of streptococcal pyrogenic exotoxin C vaccine toxoids that protective in the rabbit model of toxic shock syndrome. J. Immunol. *165*, 2306–2312.

36. Hodtsev, A.S., Choi, Y., Spanopoulou, E., and Posnett, D.N. (1998). Mycoplasma superantigen is a CDR3-dependent ligand for the T cell antigen receptor. J. Exp. Med. *187*, 319–327.

37. Ciurli, C., Posnett, D.N., Sékaly, R.-P., and Denis, F. (1998). Highly biased CDR3 usage in restricted sets of β chain variable regions during viral superantigen 9 response. J. Exp. Med. *187*, 253–258.

38. Braun, M.A., Gerlach, D., Hartwig, U.F., Ozegowski, J.H., Romagne, F., Carrel, S., Kohler, W., and Fleischer, B. (1993). Stimulation of human T cells by streptococcal 'superantigen' erythrogenic toxins (scarlet fever toxins). J. Immunol. *150*, 2457–2466.

39. Kline, B.J., and Collins, C.M. (1997). Analysis of the interaction between the bacterial superantigen streptococcal pyrogenic exotoxin A (SpeA) and the human T-cell receptor. Mol. Microbiol. *24*, 191–202.

40. Davis, M.M., Boniface, J.J., Reich, Z., Lyons, D., Hampl, J., Arden, B., and Chien, Y. (1998). Ligand recognition by $\alpha\beta$ T cell receptors. Annu. Rev. Immunol. *16*, 523–544.

41. Otwinowski, Z., and Minor, W. (1997). Processing X-ray diffraction data collected in oscillation mode. Methods Enzymol. *276*, 307–326.

42. CCP4 (Collaborative Computational Project 4). (1994). The CCP4 suite: programs for protein crystallography. Acta Crystallogr. D Biol. Crystallogr. *50*, 760–763.

43. Navaza, J. (1994). AMoRe: an automated package for molecular replacement. Acta Crystallogr. D Biol. Crystallogr. *50*, 157–163.

44. Brunger, A.T., Adams, P.D., Clore, G.M., DeLano, W.L., Gros, P., Grosse-Kunstleve, R.W., Jiang, J.S., Kuszewski, J., Nilges, M., Pannu, N.S., et al. (1998). Crystallography and NMR System: a new software suite for macromolecular structure determination. Acta Crystallogr. D Biol. Crystallogr. *54*, 905–921.

45. Roussel, A., and Cambillau, C. (1989). TURBO-FRODO. In Silicon

Graphics Geometry Partners Directory (Mountain View, CA: Silicon Graphics), pp. 77–78.

46. McRee, D.E. (1999). XtalView/Xfit—a versatile program for manipulating atomic coordinates and electron density. J. Struct. Biol. *125*, 156–165.

47. Kraulis, P.J. (1991). MOLSCRIPT: a program to produce both detailed and schematic plots of protein structures. J. Appl. Crystallogr. *24*, 946–950.

48. Esnouf, R.M. (1997). An extensively modified version of MolScript that includes greatly enhanced coloring capabilities. J. Mol. Graph. *15*, 132–134.

49. Merritt, E.A., and Bacon, D.J. (1997). Raster3D. Photorealistic Molecular Graphics. Methods Enzymol. *277*, 505–524.

50. Nicholls, A., Sharp, K.A., and Honig, B. (1991). Protein folding and association: insights from the interfacial and thermodynamic properties of hydrocarbons. Proteins *11*, 281–296.

Accession Number

The atomic coordinates of the apo and zinc-soaked forms of SpeA(C90S)-mVβ8.2 and the SpeC(H35A)-hVβ2.1 complexes have been deposited in the Protein Data Bank with accession codes 1L0X, 1L0Y, and 1KTK, respectively.